



Article

Reasoning-Based Scheduling Method for Agile Earth Observation Satellite with Multi-Subsystem Coupling

Changyuan He , Yunfeng Dong *, Hongjue Li and Yingjia Liew

School of Astronautics, Beihang University, Beijing 100191, China; hechangyuan@buaa.edu.cn (C.H.); lihongjue@buaa.edu.cn (H.L.); liewyingjia@buaa.edu.cn (Y.L.)

* Correspondence: sinosat@buaa.edu.cn; Tel.: +86-1330-102-0700

Abstract: With the rapid development of agile Earth observation satellites (AEOSs), these satellites are able to conduct more high-quality observation missions. Nevertheless, while completing these missions takes up more data transmission and electrical energy resources, it also increases the coupling within each satellite subsystem. To address this problem, we propose a reasoning-based scheduling method for an AEOS under multiple subsystem constraints. First, we defined the AEOS mission scheduling model with multi-subsystem constraints. Second, we put forward a state variable prediction method that reflects the different coupling states of a satellite after analyzing the coupling relationships between various subsystems and identifying the primary limiting coupling states for each subsystem. Third, we established the reasoning rules corresponding to the planning strategies of different coupling states of the satellite by adding two planning strategies based on the planning strategies of existing planning methods. By comparing the proposed method to three heuristic scheduling methods and a meta-heuristic scheduling method, the results show that our method has better performance in terms of scheduling results and efficiency.

Keywords: agile satellite; Earth observation; mission scheduling; multi-subsystem; knowledge reasoning; state prediction



Citation: He, C.; Dong, Y.; Li, H.; Liew, Y. Reasoning-Based Scheduling Method for Agile Earth Observation Satellite with Multi-Subsystem Coupling. *Remote Sens.* **2023**, *15*, 1577. <https://doi.org/10.3390/rs15061577>

Academic Editors: Siting Xiong, Yu Tao and Rui Song

Received: 5 February 2023

Revised: 9 March 2023

Accepted: 10 March 2023

Published: 14 March 2023



Copyright: © 2023 by the authors. Licensee MDPI, Basel, Switzerland. This article is an open access article distributed under the terms and conditions of the Creative Commons Attribution (CC BY) license (<https://creativecommons.org/licenses/by/4.0/>).

1. Introduction

Earth observation satellites (EOSs) are pivotal in environmental monitoring, disaster response, national security, etc. [1,2]. EOSs typically orbit in the low Earth orbit, however, through the satellite attitude maneuver system, the attitude of a satellite can be adjusted in order to locate the ground target that has to be captured by the satellite camera. These images are then stored in the onboard storage memory and downloaded to a ground station when the satellite passes by the ground station. When the satellite is operating, the electrical power subsystem of the satellite provides electrical energy to each component and also gains recharging electrical power from solar arrays that convert solar energy into electrical power. Some typical EOSs are IKONOS [3], PLEIADES [4], FY, and HY [5].

To carry out observation missions, the satellite's missions are scheduled and on-board actions are arranged reasonably according to the satellite's state, target location, and the ground station's location, given that the constraints are satisfied so that the satellite can observe its target and transmit the observation data back to the ground station [6,7]. Due to the advent of agile Earth observation satellites (AEOSs), more observation data can be obtained within a period of time as the satellite's maneuverability and device capabilities have been greatly improved [8,9]. An Earth observation satellite can execute more missions because its capabilities are improved with the cooperation of multiple subsystems. Meanwhile, it is accompanied by more complicated coupling relationships among subsystems as well as the scarcity of resources such as data memory and electrical energy. As a result, a new challenge is raised in terms of how to schedule the satellite mission more reasonably so that the satellite can carry out more missions while meeting the constraint requirements.

The Earth observation satellite mission scheduling problem can be solved by both heuristic scheduling methods and meta-heuristic scheduling algorithms [10]. Heuristic scheduling methods are used to design scheduling strategies for solving scheduling problems based on problem analysis and previous experience. Xie [11] proposed a temporal conflict network-based heuristic algorithm, sorted the targets using a temporal conflict network, and executed target selection and scheduling according to the order of the targets. Grasset-Bourdel [12] selected targets according to the strategy of maximizing target priority and weight acquisition, and executed the decision arrangement of the observation, attitude pointing, data transmission, and equipment switching by sequentially making different levels of decision to solve the scheduling problem. Furthermore, Wang [13] modeled the scheduling problem as a complex network, defined two factors to describe the node/target importance, and obtained the effective scheduling results based on the two factors. Wang [14] proposed a scheduling method for dynamically adjusting priority ranking based on factors such as the target weight, image quality, and satellite workload balancing. Sun [15] calculated the urgency degree and merging degree according to the task urgency, value, and observation opportunity, sorted targets by the urgency degree and merging degree, and designed four strategies of target insertion into the existing target sequence to solve the scheduling problem. Liang [16] proposed an efficient heuristic with a set of precedence rules for satellite onboard activity, which could achieve real-time planning of the onboard mission. According to the aforementioned research, heuristic methods solve scheduling problems with a definite planning strategy, giving them the advantage of high computation efficiency. However, since the scheduling strategy is commonly designed for specific conditions, it lacks adaptability to different working conditions, especially when the coupling between multiple satellite subsystems increases, which lead to different coupling states.

As for the meta-heuristic scheduling algorithms, the neighborhood space of the solution is searched according to the search rules to solve the scheduling problem. These methods obtain a good and feasible solution, but the computation time taken is comparatively long due to the iterative process. Baek [17] applied the genetic algorithm to the satellite mission scheduling problem while Liu [18] proposed a large neighborhood search algorithm for the mission scheduling of the AEOS. Du [19] proposed an ant colony algorithm based on the sensational and consciousness strategy to solve the area target observation mission scheduling problem. Furthermore, Cui [20] designed a modified ant colony optimization algorithm with tabu lists to solve the problem of video satellites for ground multi-object staring imaging. Hao [21] improved the immune clonal selection algorithm, genetic algorithm, ant colony algorithm, and particle swarm algorithm and applied them in mission scheduling. Barkaoui [22] proposed a vehicle routing problem with the time window-based hybrid genetic algorithm to tackle the single objective static multi-satellite collection scheduling problem. Zhang [23] developed an improved genetic algorithm to solve the integrated satellite imaging and data transmission scheduling problem. Zhou [24] proposed an improved adaptive ant colony algorithm to solve the scheduling problem of multiple observations with variable duration. Meta-heuristic methods can find a satisfactory solution in the solution space, however, due to the increased coupling among satellite subsystems, the computational complexity of single-stepping in the search process also increases, resulting in a more time-consuming computation.

As the planning strategy of the heuristic methods cannot be adjusted to different working conditions, knowledge reasoning methods can be introduced as an improvement. By representing knowledge and recognized rules with a knowledge base, knowledge reasoning methods are capable of judging different situations and complying with the reasoning rules to infer and obtain classification results, decision rules, and suggestions. Knowledge reasoning methods have been widely used in medical diagnosis, knowledge interpretation, motion scheduling, and other fields [25–27]. In aspects of motion scheduling and control, knowledge reasoning methods are used in robot path scheduling or control processes. Researchers have applied knowledge reasoning methods to motion scheduling

and the control of underwater robotic vehicles [28,29], four-legged robots [30], and omnidirectional robots [31]. According to the predefined reasoning rules, knowledge reasoning methods can infer the actions of a controlled object in different states based on the obtained state information.

In this paper, we researched the satellite onboard mission scheduling problem. With the real-time requirement and onboard computing resource prioritization, the scheduling algorithm is required to obtain better scheduling results with a shorter computation time. In this case, we introduced the knowledge reasoning method to tackle the mission scheduling problem of the AEOS. After classifying various coupling states according to the coupling relationships of the satellite subsystems, we established the reasoning rules to select applicable scheduling strategies in different coupling states. By using the knowledge reasoning method, the computation speed can be increased, and the adaptability of the scheduling method to different working conditions can be enhanced.

Although researchers have introduced reasoning methods to the satellite scheduling problem, our proposed method is unlike the others. Song [32] applied the reasoning method to modify the genetic algorithm and used knowledge reasoning to select the rules for various population initialization, crossover, and mutation. Conversely, our scheduling strategies were developed in accordance with different coupling states of the satellite so that the observation targets could be selected based on the satellite state. Additionally, our proposed method aims to address the mission scheduling problem for EOS while the research in [32] was for a relay satellite. Tinker [33] suggested a case-based reasoning method in the scheduling problem, whereas our proposed method is a rule-based reasoning method. The focus in [33] was on the task schedulability while we focused on addressing the mixed-integer programming problem.

In this paper, we defined the satellite multi-subsystem coupling scheduling problem and proposed a reasoning-based scheduling method (RS) for AEOS with multi-subsystem coupling. The two contributions of this study are:

1. A satellite coupling state prediction method was proposed. We analyzed the coupling relationship between satellite observation, data transmission, and electricity subsystems. Subsequently, we determined the different coupling states of AEOS with each subsystem as the main limiting factor and sorted the variables that reflected the satellite coupling states, and then proposed a state prediction method for these variables;
2. RS was established. Based on the observation-priority scheduling strategy in previous research [34,35], we proposed two planning strategies including the data transmission-priority scheduling strategy and electricity-priority scheduling strategy. We also constructed reasoning rules that corresponded to different scheduling strategies for different satellite coupling states.

The remainder of this paper is organized as follows. Section 2 defines the satellite multi-subsystem coupling scheduling problem, while Section 3 describes the satellite multi-subsystem coupling analysis process, RS, and heuristic methods. Furthermore, Section 4 presents the simulation working conditions and results. The discussion is carried out in Section 5, and Section 6 concludes this paper.

2. Problem Description

The satellite Earth observation mission studied in this paper was the observation and data transmission mission of multiple targets by an individual AEOS. The observation target type in this research was the point targets that are fixed on the Earth's surface. A single complete mission involves a satellite using a camera to capture images of a target, generating and storing the observation data, and connecting to the ground stations for data transmission, as shown in Figure 1. We defined the satellite observation mission scheduling problem as a mixed-integer programming problem.

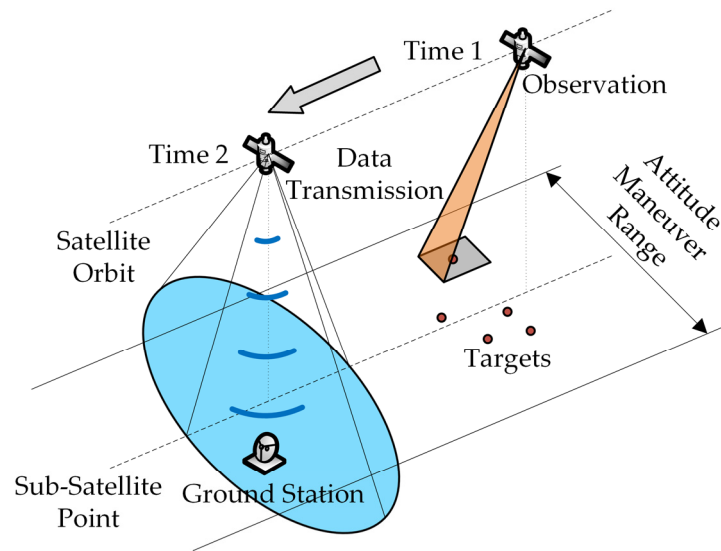


Figure 1. Schematic diagram of satellite Earth observations.

Parameters that are involved in the mission scheduling problem are shown in Table 1.

Table 1. Parameters in the problem description.

Parameter	Meaning
n_t	The number of targets
v_i	The profit of target i
t_s, t_e	The start and end time of the scheduling
Δt_o	The observation time of single target
t_{osi}, t_{oei}	The start time and the end time of the observation of target i , the relationship between them is $t_{oei} = t_{osi} + \Delta t_o$
Δt_d	The data transmission time of single target
t_{dsi}, t_{dei}	The start time and the end time of the data transmission of target i , the relationship between them is $t_{dei} = t_{dsi} + \Delta t_d$
Δt_{ds}	The device switching time between each data transmission in different time windows
$\Delta t_{Ai,j}$	The attitude maneuver time required for attitude transition of two observation missions
t_{wsi}, t_{wei}	The start time and the end time of the observation time window of target i
t_{gsk}, t_{gek}	The start time and the end time of the data transmission time window k
M, M_{\max}	M is the occupied memory capacity and M_{\max} is the total memory capacity
W, W_{\max}	W is the available electrical energy and W_{\max} is the electrical energy capacity of the battery

The decision variables are as follows:

- $x_i \in \{0, 1\}$ $i = 1, 2, \dots, n_t$ represents the decision of whether to observe target i ;
- $g_{ij} \in \{0, 1\}$ $i, j = 1, 2, \dots, n_t$ represents whether the observation of target j is after the observation of target i or not;
- $y_i \in \{0, 1\}$ $i = 1, 2, \dots, n_t$ represents whether to download the observation data of target i or not;
- $h_{ij} \in \{0, 1\}$ $i, j = 1, 2, \dots, n_t$ represents whether the download mission of target j is after the observation of target i or not.

The objective function of the problem can be expressed as

$$\max J = \sum_1^{n_t} v_i y_i, \quad (1)$$

where J is the objective function value. The objective function attempts to maximize the total profit of targets that complete an observation and data download. The target profit v_i can be described as its value to the users and its importance to the targets. The higher the profit, the more important the target. Meanwhile, profit v_i can also represent the priority of the targets. To obtain a higher objective function value, the targets with a higher profit will be prioritized when conducting observation missions.

The constraints that should be considered in the mission scheduling problem are as follows:

$$t_{osi} \geq t_{wsi} \wedge t_{oei} \leq t_{wei}, \quad (2)$$

$$t_{osj} - t_{oei} \geq \Delta t_{Ai,j} \quad g_{ij} = 1, \quad (3)$$

$$t_{dsi} \geq t_{gsk} \wedge t_{dei} \leq t_{gek}, \quad (4)$$

$$[t_{dsi}, t_{dei}] \cap [t_{dsj}, t_{dej}] = \emptyset \quad \forall 1 \leq i \leq n_t, 1 \leq j \leq n_t, y_i = 1, y_j = 1, i \neq j, \quad (5)$$

$$t_{dsj} - t_{dei} \geq \Delta t_{ds} \vee t_{dsi} - t_{dej} \geq \Delta t_{ds} \quad \forall 1 \leq i \leq n_t, 1 \leq j \leq n_t, y_i = 1, y_j = 1, i \neq j, k_{gi} \neq k_{gj}, \quad (6)$$

$$t_{dsi} \geq t_{oei}, \quad (7)$$

$$0 \leq M \leq M_{\max}, \quad (8)$$

$$0 \leq W \leq W_{\max}, \quad (9)$$

Equation (2) represents the observation time window constraint. Equation (3) represents the attitude maneuver constraint, which means that the interval between two observation missions must be greater than the attitude maneuver time required for the attitude transition of two observation missions. The calculation method of the satellite observation time window and the calculation of $\Delta t_{Ai,j}$ are introduced in Appendix A.

Moreover, the data transmission constraints consist of the data transmission time window constraint, the data transmission mission limit constraint, the data transmission equipment conversion time constraint, the observation data download logic constraint, and the memory capacity constraint, which are expressed as Equations (4)–(8). The data transmission time window constraint requires the data transmission from the satellite to ground stations to be executed within the data transmission time window, and the calculation method of the satellite data transmission time window is introduced in Appendix A. The relationship between Δt_d and Δt_o is expressed as $\Delta t_d = \frac{R_{cam}}{R_{datatrans}} \Delta t_o$, where R_{cam} is the data generation rate of the camera and $R_{datatrans}$ is the data transmission rate of downloading the data to the ground stations. The data transmission mission limit constraint limits the observation data of one target to be downloaded at the same time. The data transmission equipment conversion time constraint requires a device switching time Δt_{ds} between each data transmission in different time windows; in Equation (6), k_{gi} and k_{gj} are the serial numbers of the data transmission time windows to download the observation data of target i and target j . The observation data download logic constraint only allows the satellite to download the observation data after the data are completely stored in the memory. The memory capacity constraint is that the memory capacity occupied by all the observation data cannot exceed the maximum memory capacity. The occupied memory capacity can be calculated as follows:

$$M = \int (R_{in}t - M_{era})dt, \quad (10)$$

where R_{in} is the data generation rate, $R_{in} = R_{cam}$, during the observation periods while $R_{in} = 0$ in the spare time. M_{era} , is the erased data volume. After the satellite downloads the target observation data, the occupied memory capacity can be instantly released by erasing the downloaded observation data.

Equation (9) represents the electricity constraint, which requires the electrical energy to be greater than 0, while the electrical energy cannot exceed the electrical energy capacity of the battery. The available electrical energy can be calculated as follows:

$$W = W_{initial} + \int (P_{in}t - P_{camout}t - P_{datatransout}t - P_{normout}t)dt, \quad (11)$$

where $W_{initial}$ is the initial electrical energy of the satellite and P_{in} is the solar arrays' charging electrical power. When the satellite is operating and executing its mission, it consumes electrical energy that can be supplemented by receiving solar energy through solar arrays. The charging power of the solar arrays can be calculated as

$$P_{in} = P_{solarwing} \cos \theta, \quad (12)$$

where $P_{solarwing}$ is the charging power when the sun vector is perpendicular to the solar arrays, and can be calculated according to the solar arrays area, solar constant, photoelectric conversion efficiency, and other parameters. θ is the angle between the normal vector of the solar arrays and the sun vector. Back to Equation (11), P_{camout} is the electrical power consumption of the camera, which is equal to the camera electrical power P_{cam} during the observation periods and equal to 0 in the spare time. $P_{datatransout}$ is the electrical power consumption of the data transmission devices, which is equal to the data transmission devices' electrical power $P_{datatrans}$ during the data transmission periods while equal to 0 in the spare time. Finally, $P_{normout}$ is the electrical power consumed by the satellite under normal operation.

3. Proposed Methods

This section is divided into three subsections, where the content of each subsection is:

1. The coupling relationship between the satellite observation, data transmission, and electricity subsystems is analyzed. Next, the different coupling states where each subsystem is the main limiting factor are identified, followed by the extraction of the coupling characteristic variables reflecting different coupling states;
2. The description of the RS algorithm including the satellite state prediction, reasoning of the target selection strategies, target weight calculation, target selection, and scheduling;
3. Three heuristic scheduling methods are given on the basis of three scheduling strategies for a comparison with RS.

3.1. Multi-Subsystems Coupling Relationship Analysis of Earth Observation Satellite

According to the objective function of the scheduling problem, the more high-profit targets can be observed and downloaded, the higher the objective function value (i.e., total profit) that can be achieved. Factors that determine the total profit include the number of high-profit targets that can be observed, the number of targets that the observation data can download, and the available electrical energy that can be used for observation and data transmission. As stated in the previous section, the calculation methods for each subsystem's variable clearly show the relationship between the observation, data transmission, and electricity subsystems, as shown in Figure 2. Therefore, we first analyzed the mutual relationship among three subsystems including observation, data transmission, and electricity. The observation subsystem consists of the camera payload as well as the attitude control subsystem of the satellite. The data transmission subsystem consists of memory and data transmission devices, while the electricity subsystem comprises the batteries, solar wings, solar arrays, and electric parts of devices.

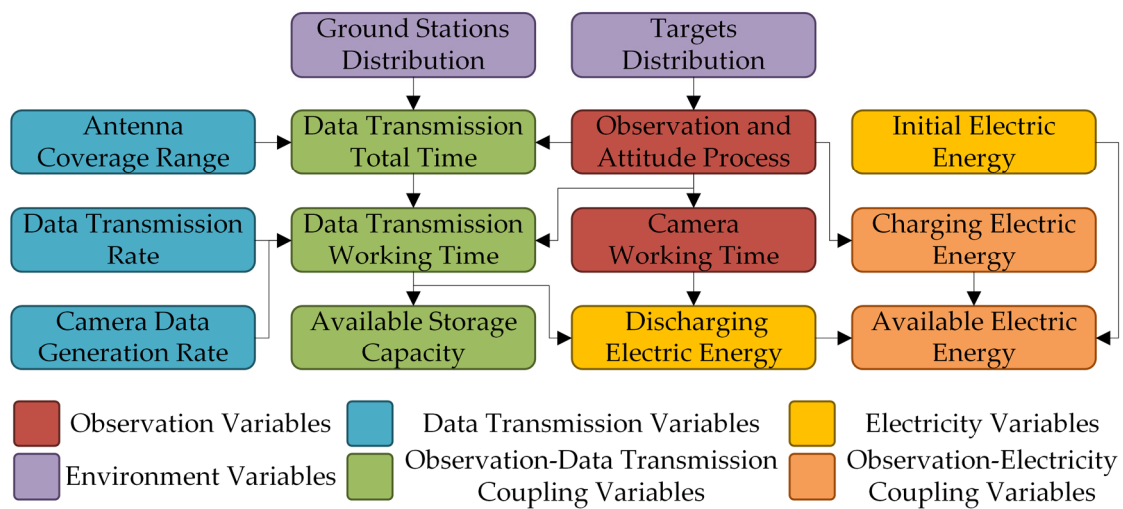


Figure 2. Coupling relationship diagram of satellite multi-subsystem variables.

To begin with, we analyzed the coupling relationship between the observation subsystem and the data transmission subsystem of the satellite. The satellite orbit used for this analysis was the same as the one used in Section 4, as shown in Table 2. The number of observable targets and the number of targets that the observation data can download jointly determine the total profit that can be obtained. There are two conditions that will result in a lesser total profit, which are (1) the number of observable targets is large and the data transmission time window available for the data download is short, and (2) the number of observable targets is small and the data transmission time window available for the data download is long. According to the calculation method of the data transmission time window in Appendix A, the length of the data transmission time window is determined by the attitude of the satellite when it flies over the ground station, and the angle between the position vector of the ground station and the satellite orbital plane, as shown in Figure 3. We plotted the surface of the length of the satellite’s data transmission time window when the satellite maintains different roll angles and the angle between the position vector of the ground station and the orbit plane is different, as shown in Figure 4.

Table 2. The satellite parameters.

Parameter Name	Parameter Value
Orbit Type	Sun-synchronous Orbit
Orbit Height	650 km
Orbit Eccentricity	0
Orbit Inclination	97.99°
Orbit Right Ascension of Ascending Node	100.348°
Orbit Argument of Perigee	0°
Attitude Maneuver Calculate Method	Trapezoidal Method
Max Attitude Maneuver Angular Velocity	1°/s
Max Attitude Maneuver Angular Acceleration	0.5°/s ²
Max Maneuvering Range Half Cone Angle α_{max}	45°
Camera’s Data Generation Rate R_{cam}	2 Gbps
Data Transmission Rate $R_{datatrans}$	1 Gbps
Antenna Coverage Half Cone Angle α_b	70°
Max Charging Electrical Power of Solar Arrays $P_{solarwing}$	1.5 kW
Camera Electrical Power P_{cam}	1 kW
Data Transmission Devices Electrical Power $P_{datatrans}$	0.5 kW
Satellite Normal Electrical Power $P_{normout}$	0.2 kW
Battery Electrical energy Capacity W_{max}	2.7×10^6 J
Single Target Observation Time Δt_0	20 s

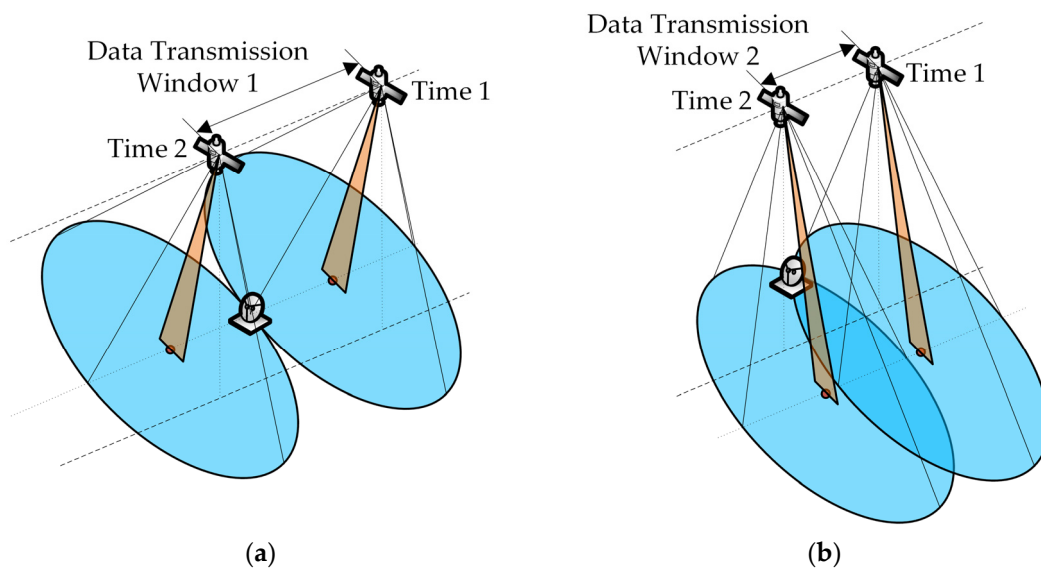


Figure 3. Schematic diagram of the data transmission window with different satellite attitudes. (a) Satellite attitude pointing to the ground station. (b) Satellite attitude not pointing to the ground station.

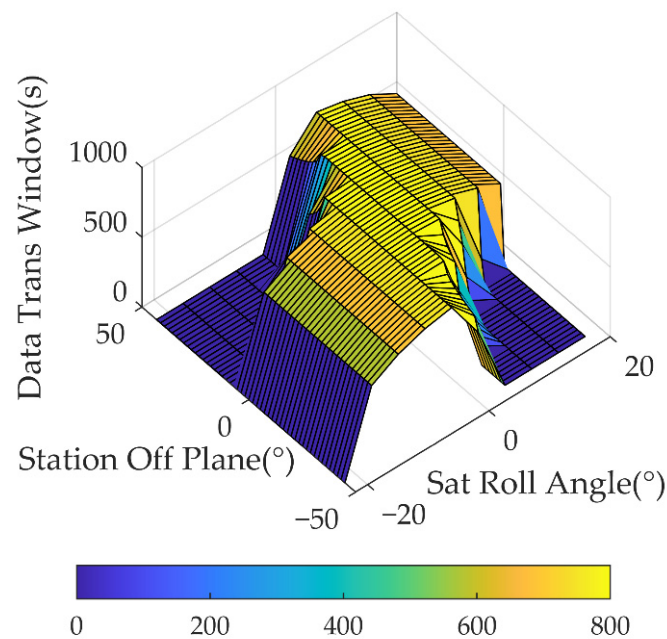


Figure 4. Influence diagram of the satellite attitudes and ground station distribution on the data transmission time.

In Figure 4, the X-axis represents the roll angle of the satellite, the Y-axis is the angle between the position vector of the ground station and the orbit plane, and the Z-axis represents the length of the data transmission time window. It can be seen from the figure that the smaller the satellite's roll angle and the closer the ground station is to the subsatellite point, the longer the data transmission time window duration that the satellite can obtain. Meanwhile, when the satellite's attitude is pointing toward a ground station, the satellite can obtain more data transmission within the time window duration. Due to this coupling relationship, some targets may be distributed far away from the ground stations, causing the satellite to have less data transmission time or no data transmission time while observing these targets. When the subsequent data transmission time and the memory capacity are sufficient, observing these targets will not affect the data recording or

downloading. In contrast, when the subsequent data transmission time or memory capacity is insufficient, the lack of data transmission time or the lack of memory capacity will result in fewer target observations and data downloads. At this time, choosing targets close to the ground stations may obtain more data transmission time and a higher total profit. Hence, this situation reflects the conflicting relationship between the observation subsystem and the data transmission subsystem. The state variables that reflect the main limiting factor between observation and data transmission includes the volume of observation data, the amount of transmission data, and the capacity of on-board memory. The observation subsystem is the main limiting factor when the data transmission time is sufficient for the data download while the memory capacity is sufficient to store observation data. In this case, the path should be scheduled to allow the satellite to perform more target observations. Conversely, when the data transmission subsystem is the main limiting factor, the path should be scheduled to enable the satellite to have more data transmission time.

Additionally, we analyzed the relationship between the observation subsystem and the electricity subsystem. The choice of observation path and the amount of satellite electrical energy determine the number of target observations. The variables that determine the available electrical energy of the satellite include the initial electrical energy satellite carriers, the electrical energy consumed by the satellite observation, data transmission, and normal operation, and the supplementary electrical energy from the solar arrays. The initial electrical energy was determined by the initial conditions, while the electrical energy consumption of the normal operation was determined by the normal electrical power consumption of the satellite. Furthermore, the electrical power consumption of the satellite observation and data transmission was determined by the number of observable targets and the amount of data transmitted. The supplementary electrical power from the satellite's solar arrays is related to the charging power of the solar arrays and also to the angle between the normal vector of the solar arrays and the Sun vector. In other words, the satellite charging electrical power is related to the choice of observation path. Then, we examined the coupling relationship between the satellite charging electrical power and the observation path by analyzing the available electrical power under different attitude conditions. We plotted the charging electrical power surface during the sunlight period in one orbital period with different roll angles, as shown in Figure 5.

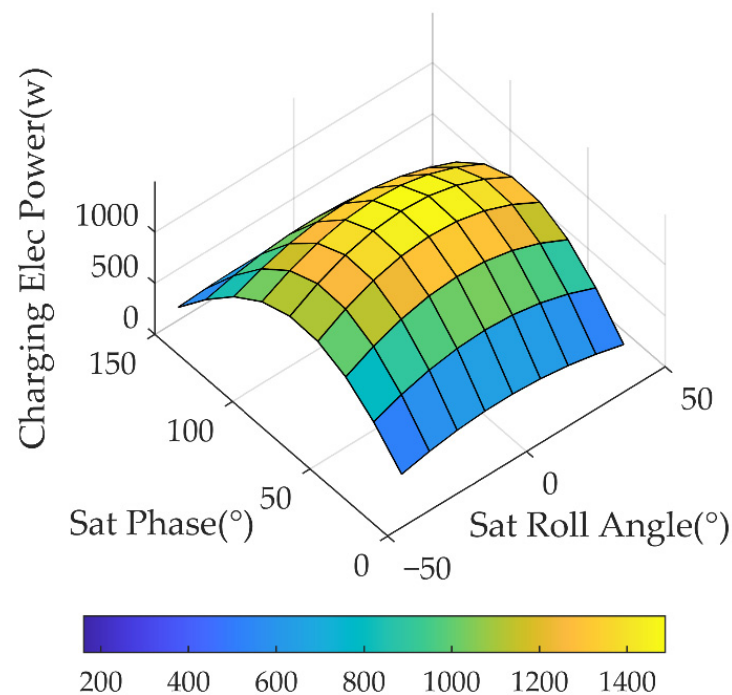


Figure 5. Influence diagram of the satellite phases and attitudes on charging power.

The X-axis in Figure 5 is the satellite's roll angle, the Y-axis represents the phase angle of the satellite's orbit, and the Z-axis is the charging electrical power. The selected orbit is a Sun-synchronous orbit, and the Sun vector is nearly parallel to the satellite's orbital plane; the normal vector of the satellite solar arrays is along the $-Z$ -axis of the satellite body coordinate system. From Figure 5, it can be clearly seen that when the normal vector of the solar arrays is nearly parallel to the Sun vector, there is more electrical power that can be gained; this is consistent with the expression of Equation (12). In some situations, some targets may appear in locations where the satellite receives less charging power while observing the targets. When there is sufficient electrical energy for the satellite, the observation of these targets will not cause a shortage in the electrical energy. However, when the supply of electrical energy is insufficient, the satellite probably cannot observe all of the targets and transmit data to the ground stations as a result of the low electrical energy supply. The satellite can obtain more electrical energy if it chooses to observe targets that are located in locations that allow more charging power to be generated. In this way, more observation and data transmission of the targets can be achieved. This reflects the conflicting relationship between the observation subsystem and the electricity subsystem. The state variable that indicates the main constraint between the observation subsystem and the electricity subsystem is the remaining electrical energy of the satellite. When the satellite's initial electrical energy and charging electrical energy are sufficient for the electrical energy consumption of devices and the observation subsystem is the main limiting factor, the path scheduling should allow the satellite to obtain more target observations. In contrast, when the electricity subsystem is the main limiting factor, the path scheduling should allow the satellite to obtain more charging electrical energy.

3.2. Reasoning-Based Scheduling Method

According to the coupling relationship between subsystems, the target selection strategy for satellites in different coupling states is different. Therefore, the scheduling framework constructed in this paper consisted of three parts: (1) satellite state prediction based on the satellite's initial state and the distribution of targets and ground stations; (2) rule-based reasoning using satellite state prediction results and obtain the targets selection strategy; (3) the observation and data transmission scheduling according to the selected target selection strategy.

3.2.1. Satellite State Prediction

Satellite state prediction is the prediction of variables that reflect different coupled states of a satellite including the electrical energy, observation data volume, available downloading data volume, and occupied memory capacity. The satellite state prediction process consists of three predictions, which are the available observation target prediction, satellite occupied memory prediction, and satellite electrical energy prediction.

Available targets \hat{x}_i are predicted through mission scheduling without data transmission and electricity constraints. The scheduling method refers to the maximum backward time slack heuristic [34,35], and the calculation steps are shown in Appendix C. The total predicted observation data volume is expressed as

$$\hat{M}_{inTotal} = \sum \hat{x}_i \Delta t_o R_{cam}. \quad (13)$$

During the satellite Earth observation, the satellite's occupied memory capacity varies constantly. When the observation data are generated and stored, they occupy more memory capacity, instead, when the data are downloaded and deleted, the occupied memory can be released. It is necessary to divide the time segment and predict the occupied memory capacity of each time segment.

Next, the entire scheduling period is divided into non-observation segments and observation segments. If there is a large time gap between two observations, this segment is regarded as the non-observation segment, which can be expressed as

$$T_{uol} = [t_{oe\hat{s}_i}, t_{os\hat{s}_{i+1}}] \quad \exists t_{os\hat{s}_{i+1}} - t_{oe\hat{s}_i} \geq f_A(A_{\hat{s}_i}, 0) + f_A(0, A_{\hat{s}_{i+1}}), 1 \leq i \leq \hat{n}_s, \quad (14)$$

where T_{uol} is the non-observation segment; l is the segment serial number; f_A is the satellite attitude maneuver angle calculation function; \hat{n}_s is the predicted number of selected targets; and \hat{s}_i is the target's serial number of the predicted observation result. In Equation (14), T_{uol} is the sufficient time interval between two observations that allows the satellite to switch to Earth-pointing mode. We set the union set of all non-observation segments as the set of non-observation segments $T_{uo} = T_{uo1} \cup T_{uo2} \cup \dots \cup T_{uon_{uo}}$, where n_{uo} is the number of non-observation segments. If the number of targets in a segment is large, that satellite will not switch to Earth-pointing mode during the observation process; this segment is defined as the observation segment. The observation segment set is the complementary set of the observation segment sets in the total scheduling period $T_o = \complement_T T_{uo}$, where $T = [t_s, t_e]$ is the total scheduling period.

In addition, the entire scheduling period was divided into data transmission segments and non-data transmission segments. We defined $status_{datatrans}^i$ as whether target i is a favorable target for data transmission, which is represented as

$$status_{datatrans}^i = \begin{cases} 1 & \exists t_{dsk} \leq t \leq t_{gek}, \mathbf{A} = \mathbf{A}_{0i}, t = t_{ti} \\ -1 & otherwise \end{cases}, \quad (15)$$

where A_{0i} is the satellite's attitude when observing the target i at the pitch angle of 0, and t_{ti} is the time when observing the target i at the pitch angle of 0. When the satellite is observing the target i with a pitch angle of 0 at the time t_{ti} , we can determine whether the data transmission window constraint is met by determining whether there is a ground station within the satellite beam coverage. If such a ground station exists, target i is a favorable target for data transmission, otherwise, target i is an unfavorable target for data transmission. Next, we formed a union set of all data transmission time windows. In a single time period of this union set, when the number of favorable targets for data transmission is greater than the number of unfavorable targets for data transmission, this period is defined as the data transmission segment and the set of data transmission segments as T_d . Non-data transmission segment set T_{ud} is the complementary set of the non-data transmission segment $T_{ud} = \complement_T T_d$.

By taking the intersection of the observation segments and the data transmission segments, we have the observation-data transmission segments $T_{od} = T_o \cap T_d$; similarly, we obtained observation-non-data transmission segments $T_{oud} = T_o \cap T_{ud}$, non-observation-data transmission segments $T_{uod} = T_{uo} \cap T_d$, and non-observation-non-data transmission segments $T_{uoud} = T_{uo} \cap T_{ud}$. Next, we combined all four types of segments into a sequence and sorted them by time, and obtained the segment sequence Seg . The status of each segment is defined as $StatusSeg_l = od, uod, oud, uoud$, where l is the serial number of the segment.

The predicted observation data volume in segment l is the observation data volume generated from the observation of predicted available targets in segment l , which is expressed as

$$\hat{M}_{in}^l = \sum \hat{x}_i \Delta t_o R_{cam} \quad t_{sl} \leq t_{oi} \leq t_{el}, \quad (16)$$

where t_{sl} and t_{el} are the start time and the end time of segment l . The predicted available download data volume in segment l is calculated as

$$\hat{M}_{out}^l = R_{datatrans}(t_{el} - t_{sl}) \quad StatusSeg_l = od \parallel uod. \quad (17)$$

The cumulative value of the occupied memory capacity can be calculated as

$$\hat{M}_{total}^l = \begin{cases} \max(\hat{M}_{in}^l - \hat{M}_{out}^l, 0) & l = 1 \\ \max(\hat{M}_{total}^{l-1} + \hat{M}_{in}^l - \hat{M}_{out}^l, 0) & l > 1 \end{cases}. \quad (18)$$

The memory state of segment l is predicted according to the cumulative value of the occupied memory capacity using the following equation:

$$StatusM_l = \begin{cases} sufficient & \hat{M}_{total}^l \leq M_{max} \\ insufficient & \hat{M}_{total}^l > M_{max} \end{cases}. \quad (19)$$

From Equation (19), we can see that when the cumulative value of the occupied memory capacity is less than the memory capacity, the memory state $StatusM_l$ is *sufficient*, else, $StatusM_l$, is *insufficient*. The predicted available download data volume of all the data transmission segments is expressed as

$$\hat{M}_{outTotal} = \sum R_{datatrans}(t_{el} - t_{sl}) \quad StatusSeg_l = od || uod. \quad (20)$$

The predicted electrical energy consumption of the mission-related devices can be calculated according to the total predicted observation time and total data transmission time. The predicted electrical energy consumption includes the electrical energy consumption of mission-related devices and the normal electrical energy consumption, which can be expressed as

$$\hat{W}_{out} = P_{cam} \left(\sum_1^{n_t} \hat{x}_i \Delta t_o \right) + P_{datatrans} \left(\sum_1^{n_t} \hat{y}_i \Delta t_d \right) + P_{normal}(t_e - t_s). \quad (21)$$

The predicted charging electrical power can be numerically calculated according to the satellite's attitude history, while the predicted charging electrical energy \hat{W}_{in} can be further calculated by integrating the predicted charging electrical power.

3.2.2. Rule-Based Reasoning and Target Weight Calculation

Mission scheduling determines the observation path through the selection of different targets. A common scheduling method is to adjust the selection order of targets by determining the weights of the targets. We assigned different weights to targets under different satellite coupling states to realize the switching of the scheduling strategy.

We described the strategy selection as the reasoning rules under different satellite coupling states and reason as the target's flags of preference including the data transmission and electricity flags. Next, we recorded the serial number of the location segment for each target as $Seg_i = l$ $t_{sl} \leq t_{ti} < t_{el}$, and the reasoning rules for the flag of preference of each target can be expressed as follows:

IF $StatusM_{Seg_i} = insufficient$ **OR** $\hat{M}_{outTotal} > \hat{M}_{inTotal}$
THEN $flag_{datatrans}^i = 1$
IF $StatusM_{Seg_i} = sufficient$ **AND** $\hat{M}_{outTotal} \leq \hat{M}_{inTotal}$
THEN $flag_{datatrans}^i = 0$
IF $W_{initial} + \hat{W}_{in} < \hat{W}_{out}$
THEN $flag_{ele} = 1$
IF $W_{initial} + \hat{W}_{in} \geq \hat{W}_{out}$
THEN $flag_{ele} = 0$

From the above reasoning rules, when the predicted memory capacity state is low or the predicted total available data transmission volume is less than the predicted total observation data volume in segment l , the target is given a flag that has more preference to data transmission $flag_{datatrans}^i = 1$, otherwise the target is given a flag that has less

preference to data transmission $flag_{datatrans}^i = 0$. When the sum of the satellite initial electrical energy and the predicted charging electrical energy is less than the predicted total electrical energy consumption, the target is given a flag that has more preference to electricity $flag_{ele} = 1$, otherwise the target is given a flag that has less preference to electricity $flag_{ele} = 0$.

The weight of targets is calculated based on the preferred flag of targets, which is defined as

$$w_i = c_o \frac{v_i \max(\Delta t_{lbS,i}^p)}{t_e - t_s} + c_d flag_{datatrans}^i status_{datatrans}^i + c_e flag_{ele} (1 - |\varphi_{power} - \varphi_i|), \quad (22)$$

where w_i is the selection weight of target i , and c_o , c_d , and c_e are the coefficients. The first item on the right side of Equation (22) is the product of the maximum backward time slack index and the target profit, where the higher the value this item has, the selection of this target enables the observation result sequence to have more backward time slack, which is more conducive to observation. Note that the calculation of the maximum backward time slack can be found in Appendix C. When $flag_{datatrans}^i = 1$, the favorable target for data transmission is given a higher weight, which is more conducive to the data transmission. In the third item of Equation (22), φ_i and φ_{power} are the roll angles at which the satellite observes target i and can obtain the maximum charging electrical power, respectively. From the coupling analysis in Section 3.1, it was noticeable that when the satellite's orbital plane was more parallel to the Sun vector, the favorable target for electricity is closer to the satellite's sub-satellite point; conversely, this target is further away from the satellite's sub-satellite point. The closer φ_i is to φ_{power} , the greater the charging electrical power satellite can obtain. When $flag_{ele} = 1$, the target that the satellite can obtain more electrical power from while observing is more conducive to the electricity.

3.2.3. Targets Selecting and Scheduling

The target selection and scheduling process primarily involves four steps: (1) select the targets based on the weight calculation results; (2) determine whether the constraints are met; (3) obtain the scheduling results including the selection and order of observation targets; and (4) calculate the other decision variables.

To provide a complete description of the RS algorithm, the target selection and scheduling were combined with the content in the previous two sections. The flowchart of the RS algorithm is shown in Figure 6 while the calculation steps are as follows:

1. Predict the satellite states according to the method mentioned in Section 3.1, and calculate the preferred flag of targets using rule-based reasoning according to the method mentioned in Section 3.2;
2. Unselected targets form a set U_u . Determine whether the sequence satisfies the attitude maneuver constraint after each unselected target is inserted at the position of the maximum sequence's backward time slack. Subsequently, select targets that satisfy the attitude maneuver constraint and form a target set that satisfy the attitude constraint U_a . The attitude maneuver constraint is stated in Equation (3), and the calculation of the insertion position of the maximum backward time slack is included in Appendix C;
3. Calculate the weights of targets in U_a according to Equation (22);
4. If the number of targets in U_a is more than 0, go to step 5, otherwise, go to step 9;
5. Take out the target with the highest weight in U_a and insert it into the current observation sequence at the maximum sequence's backward time slack position. Then, update the target observation sequence and remove the selected target from U_u ;
6. Based on the target observation sequence, calculate the satellite's attitude, data transmission time windows, the data downloading time, occupied memory capacity, and available electrical energy, the calculation method of the satellite state can be found in Appendix B;

7. Determine whether the data transmission constraints and electricity constraint are satisfied according to Equations (4)–(9). If the observation sequence does not satisfy the constraints after inserting the target, remove the target from the observation sequence and go to step 4, otherwise, go to step 8;
8. If the number of unselected targets in U_u is more than 0, return to step 2, else, go to step 9;
9. The observation sequence contains the information of x_i and g_{ij} . According to x_i and g_{ij} , calculate other decision variables and parameters including y_i , h_{ij} , t_{osi} , and t_{dsi} using the calculation method mentioned in Appendix B.

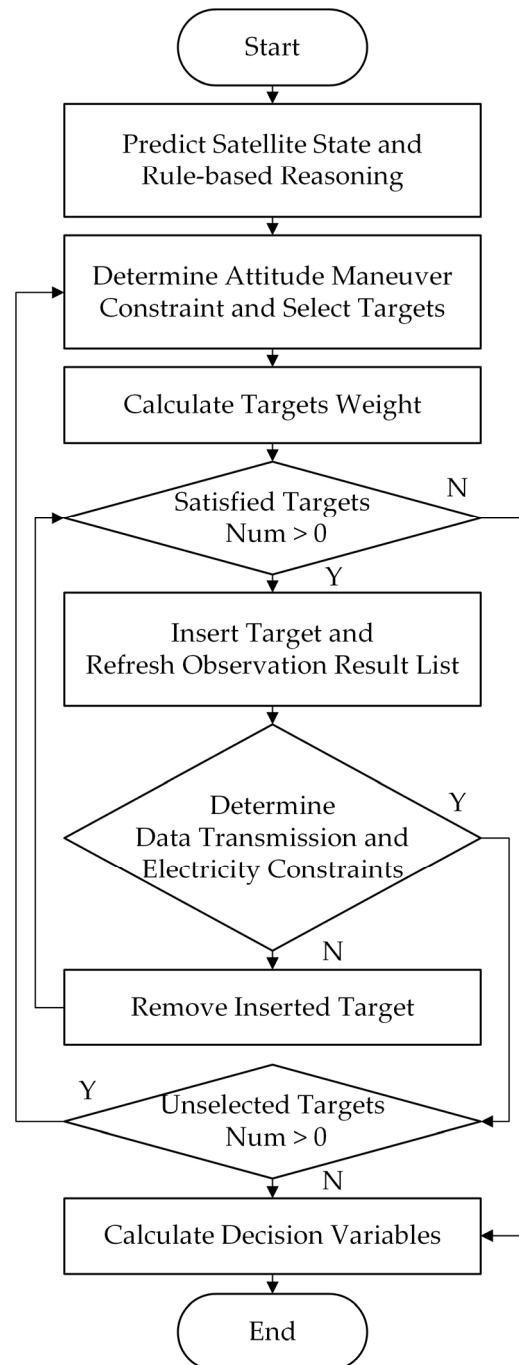


Figure 6. Flowchart of RS.

3.3. Heuristic Scheduling Methods

The heuristic scheduling methods follow the algorithm framework of RS, but without the state prediction and rule-based reasoning steps. Furthermore, the calculation of the target weight is changed to a deterministic calculation method. According to the target selection strategies mentioned in RS, three weight calculation strategies are proposed including the observation-priority strategy, data transmission-priority strategy, and electricity-priority strategy. The observation priority strategy allows the satellite to observe more targets, the data transmission-priority strategy allows the satellite to acquire more data transmission opportunities, and the electricity-priority strategy allows the satellite to obtain more charging electrical energy. Furthermore, three heuristic scheduling methods were constructed corresponding to different target selection strategies including the observation-priority heuristic algorithm (OPH), data transmission-priority heuristic algorithm (DPH), and the electricity-priority heuristic algorithm (EPH). Among all of these algorithms, OPH draws upon the existing method [34,35] using the strategy of maximum backward time slack, while DPH and EPH are two heuristic methods that we proposed based on the mission scenario analysis in this study.

The target weight calculation in OPH can be calculated as

$$w_i = \frac{v_i \max(\Delta t_{lbS,i}^p)}{t_e - t_s}. \quad (23)$$

The target weight calculation in DPH can be expressed as

$$w_i = c_o \frac{v_i \max(\Delta t_{lbS,i}^p)}{t_e - t_s} + c_d status_{datatrans}^i. \quad (24)$$

The target weight calculation in EPH can be expressed as

$$w_i = c_o \frac{v_i \max(\Delta t_{lbS,i}^p)}{t_e - t_s} + c_e flag_{ele} (1 - |\varphi_{power} - \varphi_i|). \quad (25)$$

4. Simulation Results

In this section, we compare the calculation results and time taken for different scheduling methods including RS, OPH [34,35], DPH, and EPH. At the same time, we also included the tabu search algorithm (TS) [36,37] as a conventional meta-heuristic scheduling method for comparison. We constructed four neighborhoods for the tabu search algorithm including the scheduled mission exchange neighborhood, unscheduled mission and scheduled mission exchange neighborhood, and the unscheduled mission insertion neighborhood and scheduled mission deletion neighborhood.

We then used the satellite parameters shown in Table 2 to form the simulation conditions for a comparison between the different scheduling methods; these satellite parameters can be found in [38]. Table 2 shows the orbital elements without the true anomaly and we set the true anomaly value to 120° as the satellite's initial position in all simulation conditions.

The scheduling period was set to an orbital period of 5800 s. Three groups of simulation conditions were constructed, the first group of conditions contained a satellite that had enough data transmission resources and initial electrical energy, the second group of conditions contained a satellite that had sufficient initial electrical energy but was short of data transmission resources, and finally, the third group of conditions contained a satellite with enough data transmission resources but lacked the initial electrical energy. Each group contained ten conditions in which randomly distributed target points were assigned random values within a given range. The condition parameters are shown in Table 3.

Table 3. Condition parameters.

Parameter Name	Group 1	Group 2	Group 3
Initial Electrical energy $W_{initial}$	2×10^6 J	2×10^6 J	2×10^5 J
Memory Capacity M_{max}	1200 Gbit	1200 Gbit	1200 Gbit
Target Number n_t	55	60	55
Target Distribution Area Number	2	3	2
Target Number in Each Area	15; 40	25; 15; 20	15; 40
Sub-satellite Point Phase Range of Target Distribution ($^\circ$)	[9.3, 62.1]; [9.3, 62.1]	[12.4, 55.9]; [12.4, 55.9]; [62.1, 99.3]	[62.1, 124.1]; [62.1, 124.1]
Angle Range between Targets and Orbital Plane ($^\circ$)	[−0.5, 0.5]; [4.2, 6.2]	[−5.1, −2.1]; [2.1, 5.1]; [0, 2.1]	[−0.5, 0.5]; [4.2, 6.2]
Max Target Value v_{imax}	1	1	1
Min Target Value v_{imin}	0.9	0.9	0.9

The calculation program was executed on a computer with an intel Core i7-10700@2.9 GHz CPU. The scheduling result of the OPH was used as the initial scheduling result for the tabu search algorithm. The maximum number of iterations of the tabu search algorithm was set as 500. When the historical optimal value was achieved, the calculation time taken was recorded. The coefficients in Equations (22), (24), and (25) were $c_o = 1$, $c_d = 1$, and $c_e = 1$.

The comparison of the scheduling results of the three groups of conditions are shown in Figure 7, and the results are listed in Table 4. It is obvious that TS achieved the best scheduling results among all of the methods under different conditions. The objective function value J of TS then served as a baseline for comparison with other methods. From the first group of results, it was noticeable that OPH and RS had better results when the data transmission time windows, memory capacity, and electrical energy were enough, the objective function value J was 96% of TS, and the results of DPH and EPH were worse as both had the objective values J of 88% and 74% of TS. Moreover, it can be seen from the second group of results that DPH and RS had better results when the data transmission time windows were short, and their objective function value J was 98% of TS, while the results of OPH and EPH were worse in which the objective values J were 88% and 80% of TS. From the third group of results, EPH and RS clearly had better results when the electricity energy was low as the objective function value J was 92% of TS. In contrast, the results of OPH and EPH were worse as their objective values J were 74% of TS.

The calculation time of different methods in the three groups of conditions are shown in Table 5. Since TS is an iterative algorithm, the calculation time taken is much longer than RS and the heuristic scheduling methods. The average number of iterations for TS to achieve the optimal solution in the three group of conditions was 87, 239, and 249, respectively.

A single condition from each of the three groups of conditions was chosen for analysis. The target selection and observation path of one of the conditions in the first group are shown in Figure 8. In the figure, the black circles represent the position of targets, the gray lines are the observation time windows, the blue areas are the areas where targets can be favorable targets for data transmission, and the different colored lines indicate the attitude maneuver paths and observation paths of the satellite. The paths and target points are represented with time and roll angle of the satellite instead of latitude and longitude, which can reflect the satellite observation process more intuitively.

It can be seen that the available memory capacity and electrical energy are in sufficient states during the satellite observation process from Figures 9 and 10. From Figure 8, it is clear that DPH and EPH do not select targets in an observation-priority way and thus gain fewer observations, resulting in a lower objective function value J . In contrast, RS selects targets according to OPH's strategy and performs more target observations, resulting in a higher objective function value J .

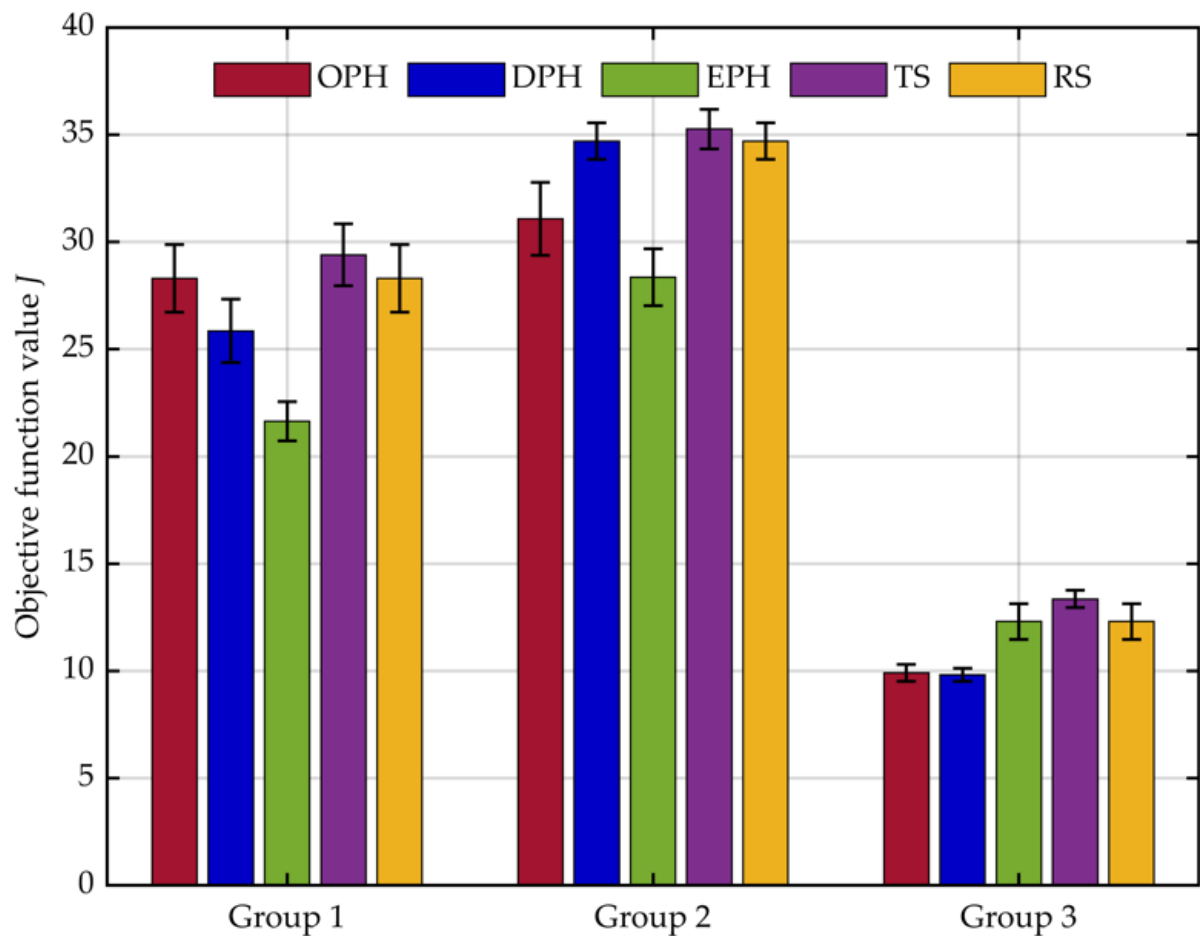


Figure 7. Comparison results of different methods.

Table 4. Resulting values of different methods.

Method	Group 1			Group 2			Group 3		
	Max	Min	Avg	Max	Min	Avg	Max	Min	Avg
OPH [34,35]	31.13	26.52	28.30	33.85	29.35	31.07	10.67	9.67	9.91
EPH	27.63	22.75	25.85	35.90	33.62	34.70	10.67	9.67	9.82
DPH	22.67	19.68	21.64	30.35	26.17	28.36	14.12	11.24	12.30
TS [36,37]	31.23	27.48	29.40	36.90	34.00	35.26	14.23	12.56	13.35
RS	31.13	26.52	28.30	35.90	33.62	34.70	14.12	11.24	12.30

Table 5. The average calculation time of different methods in different groups.

Conditions	OPH [34,35]	DPH	EPH	TS [36,37]	RS
Group 1 (s)	10.21	9.41	8.05	854.23	10.21
Group 2 (s)	15.62	12.1	15.08	3243.05	12.06
Group 3 (s)	12.96	12.97	12.82	6896.81	12.83

The target selection and observation path of a single condition in the second group are shown in Figure 11. Note that Figures 12 and 13 show that the available memory capacity and electrical energy were sufficient during the satellite observation process. As can be seen in Figure 11, DPH, TS, and RS selected favorable targets for data transmission, so they obtained more data transmission time windows. In Figure 14, the red strips are the observation periods, the yellow strips are the data download periods, and the blue strips are the data transmission time windows. It is apparent that DPH, RS, and TS obtained more

data transmission time windows. Therefore, more targets are downloaded and a higher objective function value J is obtained.

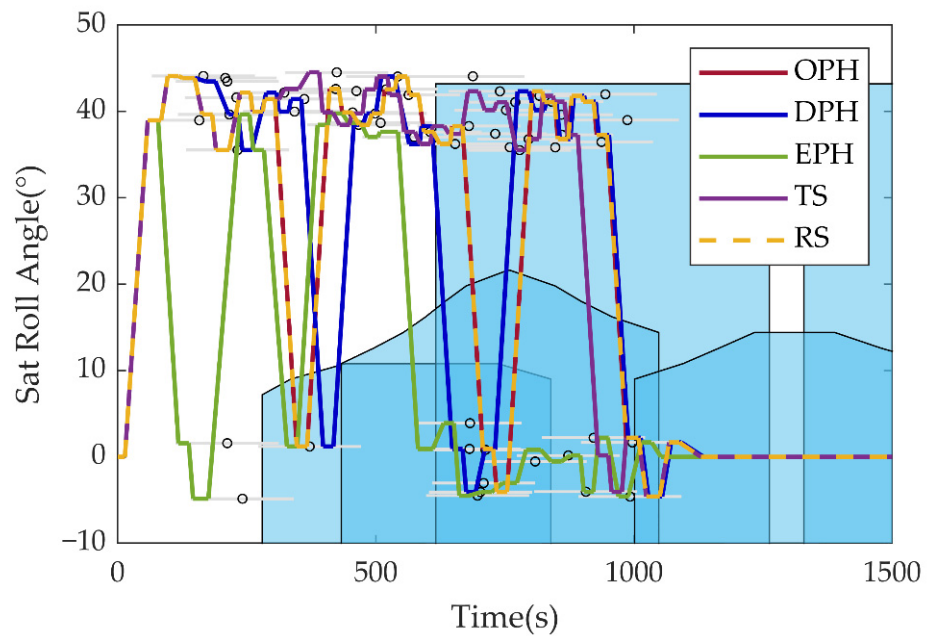


Figure 8. Targets selection and observation path diagram of a single condition in the first group.

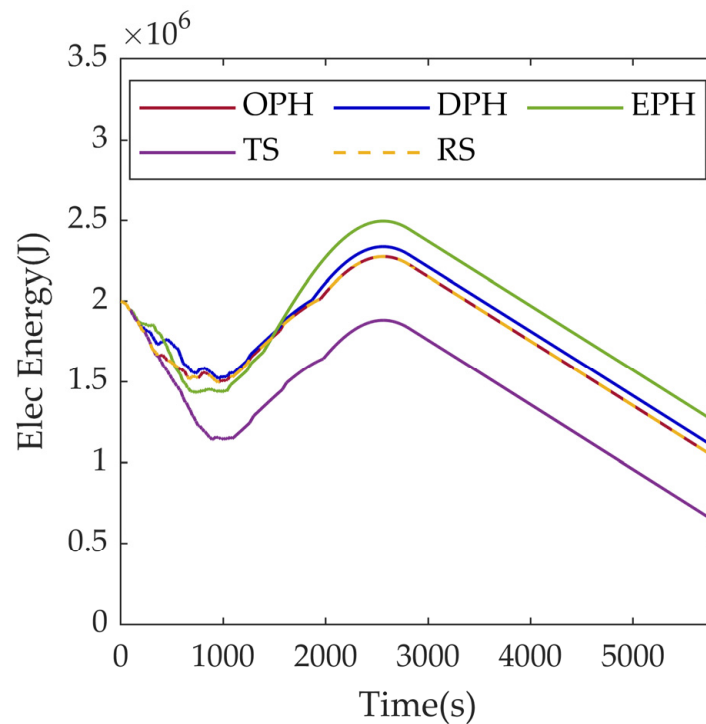


Figure 9. Satellite electrical energy diagram of a single condition in the first group.

Likewise, Figure 15 shows the target selection and observation path of a condition in the second group. It can be seen that the available memory capacity was sufficient but was deficient in electrical energy during the satellite observation process from Figures 16 and 17. From Figure 18, EPH, TS, and RS chose more targets that could obtain more electrical charging energy. Consequently, these three algorithms were capable of completing more observations (as shown in Figure 15) and data downloads, thus achieving higher objective function values.

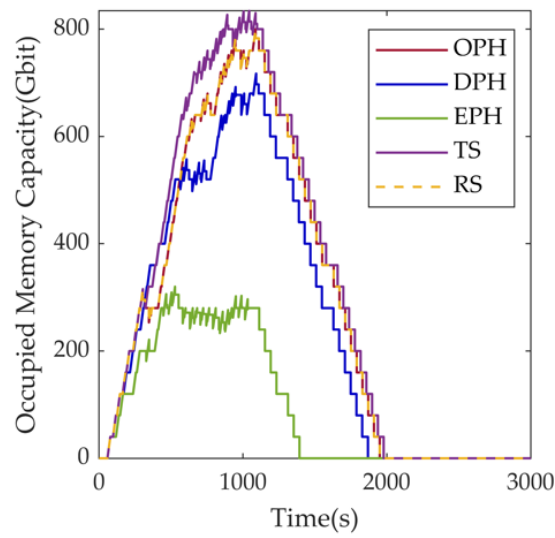


Figure 10. Satellite occupied memory capacity diagram of a single condition in the first group.

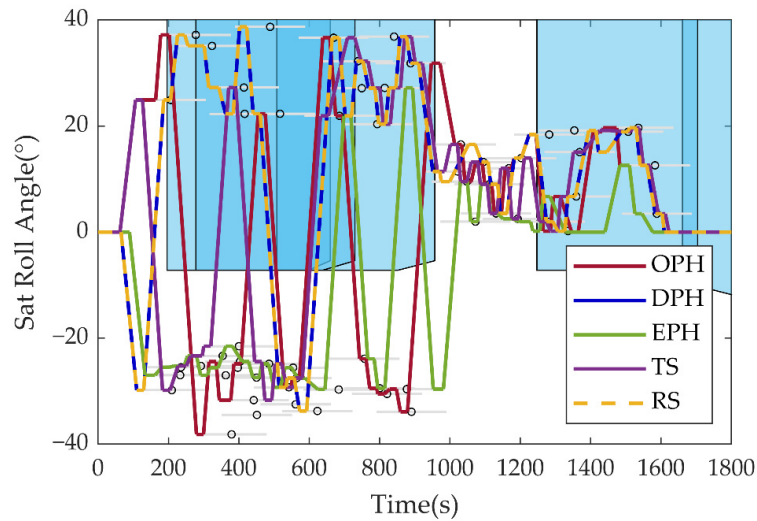


Figure 11. Targets selection and observation path diagram of a single condition in the second group.

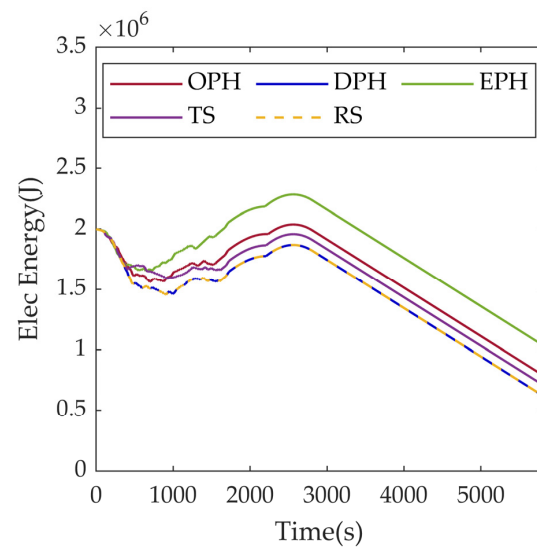


Figure 12. Satellite electrical energy diagram of a single condition in the second group.

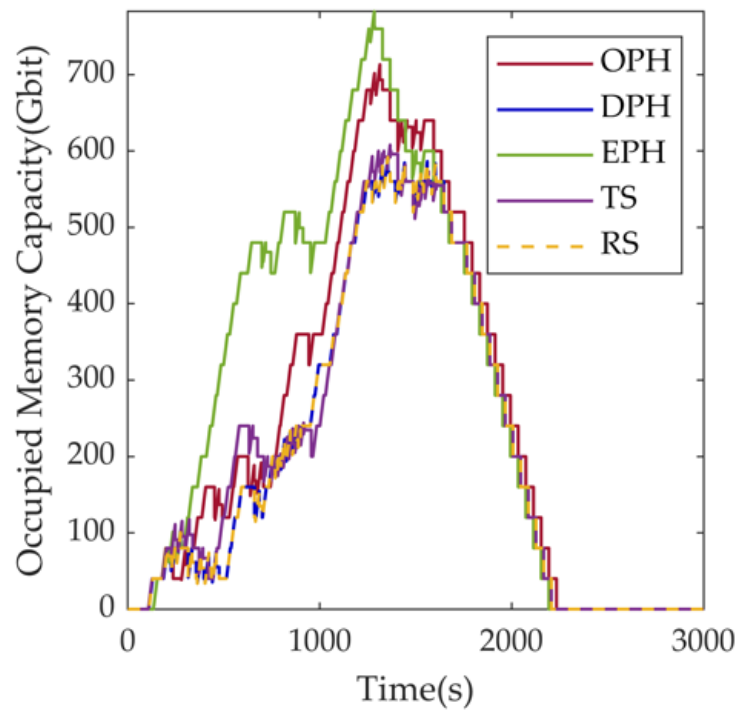


Figure 13. Satellite occupied memory capacity diagram of a single condition in the second group.

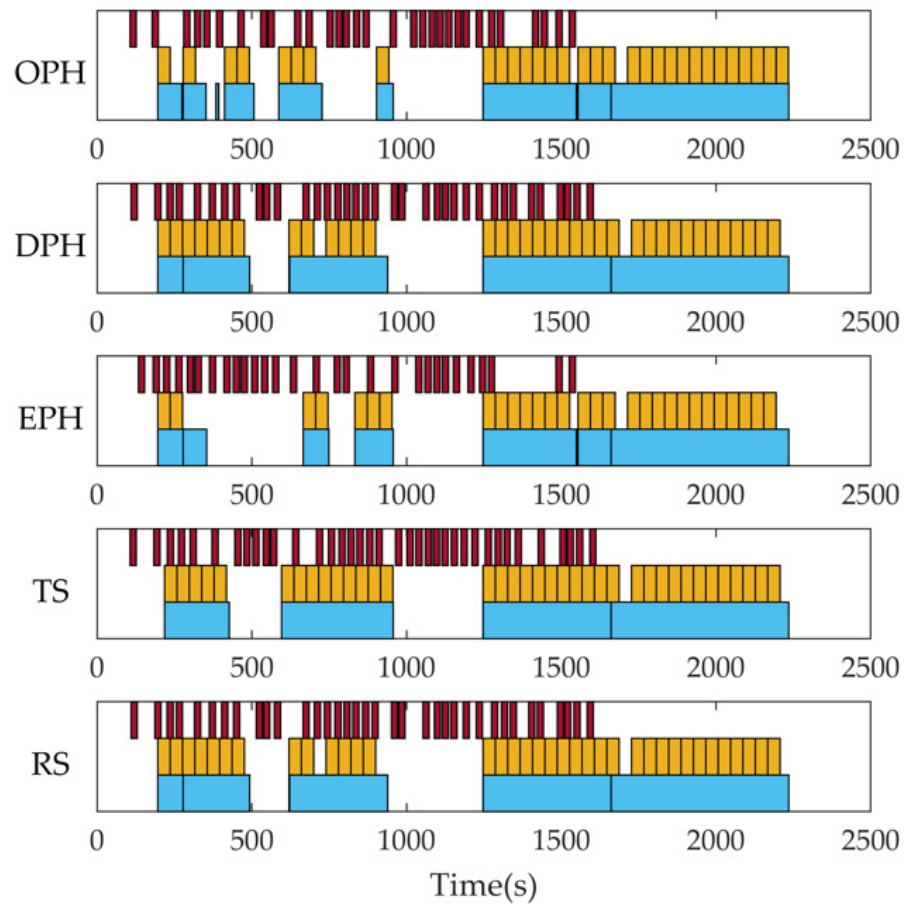


Figure 14. Observation and data transmission time period diagram of a single condition in the second group.

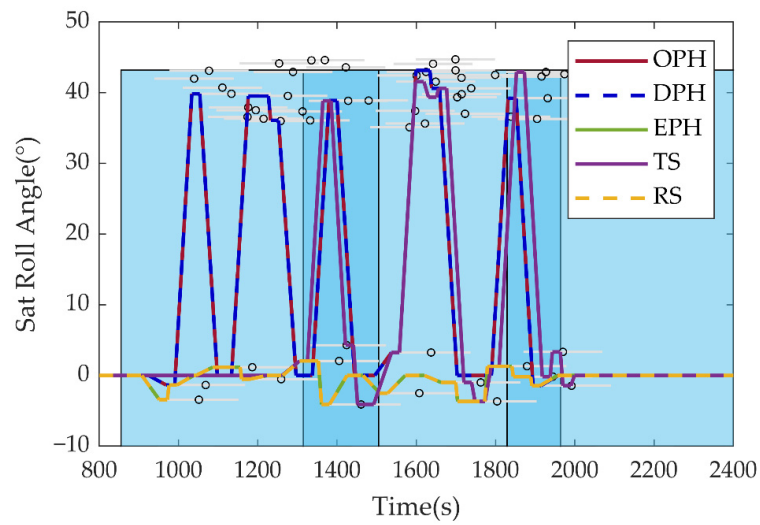


Figure 15. Targets selection and observation path diagram of a single condition in the third group.

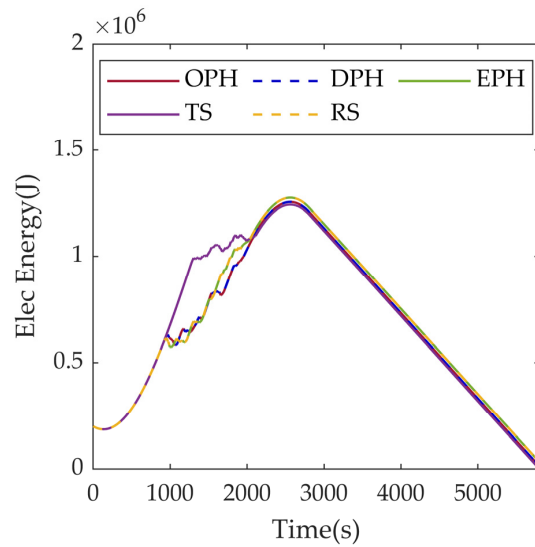


Figure 16. Satellite electrical energy diagram of a single condition in the third group.

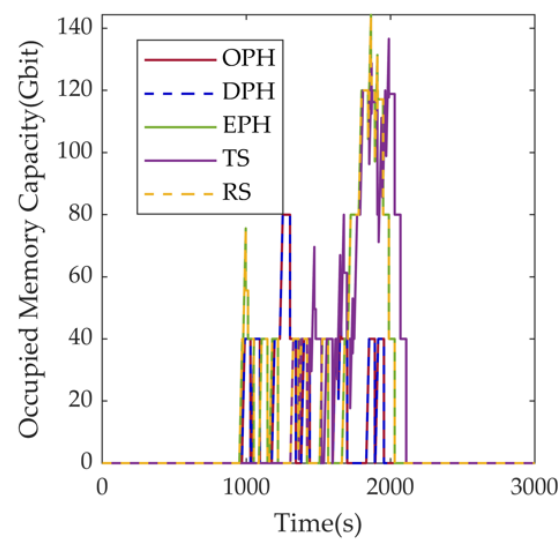


Figure 17. Satellite occupied memory capacity diagram of a single condition in the third group.

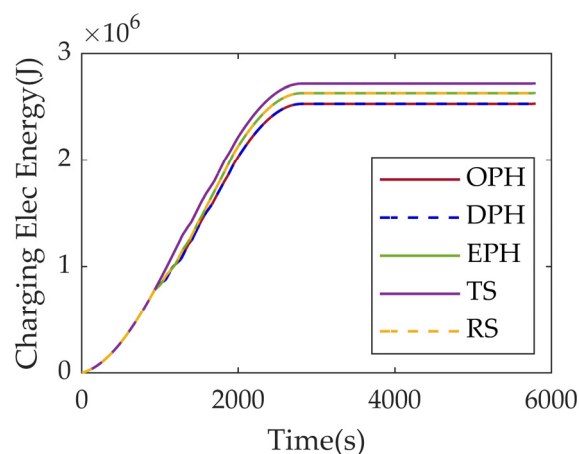


Figure 18. Charging electrical power chart of a single condition in the third group.

5. Discussion

By comparing the objective function value J for all methods mentioned in the previous section, OPH had better results under the conditions of having enough data transmission time, memory capacity, and electrical energy, but had poorer performance when there was a lack of data transmission time and electrical energy; the ratios of the resulting values of OPH to TS in the three groups of conditions (the conditions are mentioned in Table 3) were 96%, 88%, and 74%, respectively. DPH worked better when it had a lack of data transmission time, but worse with the other two groups of conditions as the ratios of the resulting J values to TS in the three groups of conditions were 88%, 98%, and 74%, respectively. Additionally, EPH had a more favorable performance when electrical energy was deficient, but not in the other two groups of conditions, as the proportions of its resulting J values to TS were 74%, 80%, and 92%, respectively. In contrast, RS outperformed the other three methods as its ratios of the resulted objective function value J to those of TS were 96%, 98%, and 92%, respectively, under the three groups of conditions. In short, RS worked well under all different conditions, whereas the heuristic methods only performed better under suitable conditions. Under appropriate conditions, the heuristic methods and RS performed similarly, as the ratio of their resulting J value to TS was about 96%. However, with unsuitable conditions, the results of RS were roughly 16% higher than those of the heuristic methods. Under all conditions, RS produced an objective function value of J that was nearly 11% higher than the heuristic scheduling methods.

From the analysis of the results of a single condition of each group, the reason behind the poor results obtained by the heuristic methods is that the main scheduling limitation factors were different in different coupling states of the satellite. Therefore, targets with higher profit should be selected when data transmission resources and electrical energy are sufficient. The satellite should also try to obtain more data transmission resources and electrical charging energy when the data transmission resources or electrical energy are limited. These match the coupling analysis results in the paper.

From the simulation results, even though group 2 was a more constrained scenario, the objective function values were slightly higher for group 2 than group 1. This is because the distribution area of targets in group 2 was larger than that in group 1, which provided more observation opportunities. Therefore, under the working conditions of group 2, even though the data transmission segments were insufficient, the amount of observation data that can be downloaded was higher than group 1, and the objective function value for group 2 was higher than that of group 1.

In all cases, although TS surpassed all heuristic methods, the calculation time taken is long due to its iterative property. The average calculation time of the heuristic methods and RS were about 12 s, whilst the average calculation time of TS was around one hour.

With good scheduling results and high computational efficiency, the RS we proposed can be applied to scenarios with limited computing resources and real-time requirements such as satellite autonomous mission scheduling, emergency scheduling, and so on.

The research in this paper can be further extended in the following aspects:

1. A potential direction is to apply the method to more different conditions, with the purpose of supplementing the knowledge base in the reasoning process according to the simulation results, and modifying the parameters;
2. Simulations can be carried out on a finer-grained component level that is closer to a real satellite. This includes the operation simulation for different satellite components, the simulation of observation data generation and transmission, and the simulation of the power consuming processes of the components. According to a finer-grained simulation condition, the simulation results can be utilized to improve the scheduling algorithm;
3. Research can be conducted on mission allocation and resource distribution for multiple satellites and orbits. Scheduling on more orbits will bring target observation opportunities in different orbit periods, reduce the pressure of observation and data transmission missions on a single orbit by selecting targets in different orbits, and hence obtain more profits. It is also crucial to perform research on how to coordinate limited resources among multiple satellites to obtain better multi-satellite mission scheduling results;
4. Targets can be merged in the preprocessing step. When the field of view of the satellite's camera is relatively wider and the distances between targets are shorter, multiple targets can be observed with a single observation. If this merging preprocess needs to be integrated into our proposed method, the neighboring targets are required to be grouped according to their satellite orbits and the frame widths of the camera in the target preprocessing step. The roll angle, time window, and scanning time duration also need to be calculated so that these grouped targets can be added to the methodological framework proposed in this paper.

6. Conclusions

To address the mission scheduling problem of multi-subsystem coupling in the process of AEOS Earth observations, RS for AEOS with multi-subsystem coupling was proposed in this paper. This method solves the scheduling problem through state prediction and scheduling strategy reasoning. From the analysis of a single condition, it can be deduced that the RS we proposed can realize the selection of a suitable scheduling strategy according to different coupling states. The selected scheduling strategy also obtained a better objective function value J , which embodies the role of knowledge reasoning in the scheduling method. Compared with the heuristic methods, RS gained a better scheduling result while having the same calculation time. Through a comparison with the meta-heuristic method (TS), RS could obtain a solution close to that of the meta-heuristic method with a significant reduced calculation time. Overall, RS had good calculation results and high computation efficiency in scheduling Earth observation missions of AEOS with multi-subsystem coupling.

Author Contributions: Conceptualization, Y.D. and C.H.; Methodology, C.H.; Software, C.H.; Validation, C.H., H.L. and Y.L.; Formal analysis, H.L. and Y.L.; Investigation, C.H.; Resources, C.H.; Data curation, C.H.; Writing—original draft preparation, C.H.; Writing—review and editing, H.L. and Y.L.; Visualization, C.H. and H.L.; Supervision, Y.D. and H.L.; Project administration, C.H.; Funding acquisition, Y.D. All authors have read and agreed to the published version of the manuscript.

Funding: This research received no external funding.

Data Availability Statement: The data used to support the findings of this study are available from the corresponding author upon request.

Acknowledgments: This work was partially supported by the Key Laboratory of Spacecraft Design Optimization and Dynamic Simulation Technologies, Ministry of Education.

Conflicts of Interest: The authors declare no conflict of interest.

Appendix A. Time Window Calculation Method

The satellite needs to aim its camera to the target so that the target is within the view of field through attitude maneuver and then maintain the attitude for push-broom imaging while observing the target. The start time and the end time of the observation can be calculated as

$$\begin{cases} t_{osi} = t_{oi} - \Delta t_o / 2 \\ t_{oei} = t_{oi} + \Delta t_o / 2 \end{cases} \quad (\text{A1})$$

where the moment when the optical axis of the satellite camera is aligned with the target is t_{oi} and the satellite observation time is a fixed value Δt_o . The satellite studied in this paper is an AEOS that can perform attitude maneuvers around the roll and pitch axes. This allows the satellite to observe the target at different moments when it is visible. The time period when the target is observable by the satellite is the observation time window. The visibility condition requires that the target be visible to the satellite, without being blocked by the Earth. Meanwhile, it also requires the satellite to satisfy the satellite attitude cone angle constraint when pointing at the target. The satellite attitude cone angle constraint is that the angle α_c between the Z-axis of the satellite body coordinate system and the Z-axis of the orbit coordinate system must not be greater than the maximum allowable half cone angle α_{cmax} during the operation period, which is

$$\frac{(\mathbf{r}_{ti} - \mathbf{r}_{ri}) \cdot (-\mathbf{r}_{ri})}{|\mathbf{r}_{ti} - \mathbf{r}_{ri}| |\mathbf{r}_{ri}|} \leq \alpha_{cmax}, \quad (\text{A2})$$

where \mathbf{r}_{ri} is the satellite position vector in the inertial coordinate system, and \mathbf{r}_{ti} is the target position vector in the inertial coordinate system, whereas the observation time window $[t_{wsi}, t_{wei}]$ can be calculated through state propagation. In this paper, each only scheduling considers the scheduling period within one orbital period; if the scheduling period is more than one orbital period, the scheduling of subsequent orbital periods can employ this method repeatedly. In the meantime, targets that are not visible during the scheduling period are not considered. These invisible targets are judged and eliminated before scheduling, therefore, the number of observation time windows n_t corresponds to the number of targets.

$\Delta t_{A_{i,j}}$ is the attitude maneuver time between the observation of target i and target j . In this paper, the camera was installed along the +Z-axis of the satellite body coordinate system, and the satellite observation attitude $A_i = [\varphi_i, \theta_i, \psi_i]$ was the Euler angle of the satellite camera's optical axis pointing to target i at t_{oi} . The attitude maneuver time can be computed as $\Delta t_{A_{i,j}} = f_t(A_i, A_j)$, where f_t is a function for calculating the attitude maneuver time according to the current attitude A_i and the next attitude A_j of the satellite.

When a satellite establishes a data connection link to a ground station for data transmission, the satellite antenna and ground station should be visible to one another. Antennas that are commonly used on satellites include shaped-beam antennas and rotatable spot beam antennas. The beam angle of rotatable spot beam antenna is small, but the coverage can be increased by rotating the antenna pointing, and the sum of rotation range and beam angle is equivalent to the antenna coverage beam angle. As for the shaped-beam antenna, it is non-rotatable and has a larger beam angle, in which this beam angle is the antenna coverage angle that is defined as α_b . The conditions for a satellite antenna and a ground station to be visible to each other include that the ground station is covered by the coverage angle of satellite antenna and the satellite position meets the minimum elevation angle requirements of the ground station, which can be expressed as

$$\alpha_r \leq \alpha_b \wedge \alpha_s \leq 90^\circ - \alpha_e, \quad (\text{A3})$$

where $\alpha_r = \arccos\left(\frac{\mathbf{r}_{rsb} \cdot \mathbf{v}_{rzb}}{|\mathbf{r}_{rsb}| |\mathbf{v}_{rzb}|}\right)$ is the angle between \mathbf{v}_{rzb} (Z-axis vector of the satellite body coordinate) and \mathbf{r}_{rsb} (the vector from the satellite to the ground station), and α_e represents the minimum elevation angle of a ground station. The data transmission time window $[t_{gsk}, t_{gek}]$ can be calculated through state propagation, $1 \leq k \leq n_g$, where n_g is the number of data transmission time windows.

Appendix B. Decision Variables Calculation Method

The observation start time t_{si} of the target can be calculated according to the selected targets x_i and observation order g_{ij} , using the calculation method in [34,35]. Calculate the ready time t_{pi} of each observation mission according to the scheduling observation list result, which can be defined as

$$t_{pi} = t_{oei-1} + \Delta t_{Ai-1,i}, \tag{A4}$$

where t_{pi} is the earliest possible start time after the completion of the previous observation mission and attitude maneuver without considering the time window. Since observing a target as early as possible within the observation time window can give subsequent targets more opportunities to be observed, and the earliest observation time can be regarded as the start observation time. The observation start time t_{osi} of target i can be expressed as

$$t_{osi} = \max(t_{pi}, t_{wsi}), \tag{A5}$$

where obtaining the larger value either from the ready time or the observation starting time. The selection of the target's data download y_i , download order h_{ij} , and download start time t_{dsi} can be calculated according to whether the targets are observed x_i and the order of observations g_i . Since no profit can be obtained as the observation data cannot be downloaded, the data download of the observed targets should be ensured, which can be expressed as

$$y_i = x_i \quad 1 \leq i \leq n_t. \tag{A6}$$

Targets where the data cannot be downloaded will not be added to the observation sequence. The order of data downloading follows the order of observations, which is

$$h_{ij} = g_{ij} \quad y_i = 1, 1 \leq i \leq n_t. \tag{A7}$$

Since the earlier data have been downloaded, the earlier downloaded data can be erased, leaving more spare memory for the observation data of subsequent targets. Hence, we arranged the data download start time at the earliest time that satisfies the data transmission constraints.

The calculation steps of the data transmission time are as follows:

1. Calculate the satellite's attitude progress based on the current satellite observation target scheduling result list. Then, calculate the start time t_{gsk} and end time t_{gek} of the data transmission time windows, and sort the data transmission time windows according to start time t_{gsk} . Attitude progress can be calculated as follows:

$$A = \begin{cases} A_i & t_{osi} \leq t \leq t_{oei} \\ A_i & f_i(A_i, 0) + f_i(0, A_{i+1}) > t_{osi+1} - t_{oei}, t_{oei} < t \leq t_{osi+1} - f_i(A_i, A_{i+1}) \\ f_A(A_i, A_{i+1}, t - (t_{osi+1} - f_i(A_i, A_{i+1}))) & f_i(A_i, 0) + f_i(0, A_{i+1}) > t_{osi+1} - t_{oei}, t_{osi+1} - f_i(A_i, A_{i+1}) < t < t_{osi+1} \\ 0 & f_i(A_r, 0) + f_i(0, A_{r+1}) \leq t_{osi+1} - t_{oei}, t_{oei} + f_i(A_r, 0) \leq t \leq t_{osi+1} - f_i(0, A_{r+1}) \\ f_A(A_i, 0, t - t_{oei}) & f_i(A_i, 0) + f_i(0, A_{i+1}) \leq t_{osi+1} - t_{oei}, t_{oei} < t < t_{oei} + f_i(A_i, 0) \\ f_A(0, A_{i+1}, t - t_{osi+1} + f_i(0, A_{i+1})) & f_i(A_i, 0) + f_i(0, A_{i+1}) \leq t_{osi+1} - t_{oei}, t_{osi+1} - f_i(0, A_{i+1}) < t < t_{osi+1} \end{cases} \tag{A8}$$

where f_A is the satellite attitude maneuver angle calculation function. The satellite attitude angle can be calculated using the current attitude angle, target attitude angle, and a calculating time (i.e., it can be a moment during attitude maneuver or after attitude maneuver is completed). Earth-pointing mode is the operation mode when there is no mission. If the time between the current observation mission and next observation mission is not enough for the satellite to turn to the Earth-pointing attitude

and then turn to the next target observation attitude, the satellite will then maintain the attitude for a set period of time before maneuvering to the next target observation attitude. If the time between the current observation mission and the next observation mission is enough to turn to the Earth-pointing attitude and then turn to the next target observation attitude, the satellite will first turn to the Earth-pointing attitude, and maintain the attitude for a certain time, and then turn to the observation attitude of the next target;

2. Select an observation target s_i according to the order of the observation result sequence. Targets are categorized into selected targets and unselected targets according to $x_i = 1$ and $x_i = 0$, and the observation target sort sequence $S = \{s_i | 1 \leq i \leq n_s\}$ is the sequence of the selected target serial numbers sorted according to the order of observation targets g_{ij} , where n_s is the number of selected targets, and s_i is the serial number of a target;
3. Start with $k = 1$, then select the k th data transmission time window and calculate the available time segment $[t_{gusk}, t_{guek}]$ of the data transmission time window that satisfies the data transmission constraints, which can be expressed as

$$[t_{gusk}, t_{guek}] = [t_{gsk}, t_{gek}] \cap [t_{oei}, t_e] \cap \mathbb{C}_T \left([t_{gcs1}, t_{gce1}] \cup [t_{gcs2}, t_{gce2}] \cup \dots \cup [t_{gcsn_g}, t_{gcen_g}] \right), \quad (A9)$$

where t_{gcsk} and t_{gcek} are the start time and end time of the occupied segment of the data transmission time window k .

4. Determine whether the available time segment $[t_{gusk}, t_{guek}]$ of the k th data transmission time window is sufficient for downloading the observation data of target s_i . If there is enough time, the data transmission start time t_{dsi} is the start time t_{gusk} . Otherwise, set $k = k + 1$, and repeat the calculation of the available time segment and download the time judgement. If there is not enough time for data downloading in all of the data transmission time windows, the data transmission constraints are not satisfied. Hence, the data transmission time calculation is ended;
5. Repeat Steps 2 to 4 until the data download time calculation of all the observation targets are completed. The targets' observation data download time can be calculated and the data transmission constraints can be judged at the same time.

Appendix C. Maximum Backward Time Slack Heuristic Scheduling Method

The calculation steps of the maximum backward time slack heuristic scheduling method [34,35] are as follows:

1. Calculate the backward time slack of each target. For a target sequence (i, \dots, j) , the backward time slack of the observation of target i is the time that i can move backward without violating the observation time window constraint and the attitude maneuver constraint, which can be calculated by the back-forward iteration as

$$\Delta t_{bi}^j = \begin{cases} t_{wei} - t_{oei} & i = j \\ \min(\Delta t_{bi+1}^j + t_{osi+1} - t_{pi+1}, t_{wei} - t_{oei}) & i < j \end{cases} \quad (A10)$$

The sequence's backward time slack is the minimum backward time of all selected targets, which can be defined as

$$\Delta t_{lBS} = \min(\Delta t_i^{j_{ns}}) \quad i = j_1, \dots, j_{ns}, \quad (A11)$$

where sequence $S = \{j_1, j_2, \dots, j_{ns}\}$. Calculate the backward time slack of target i after target i is inserted at position p , which is

$$\Delta t_{bS,i}^p = \begin{cases} \min(t_{wei} - t_{oei}, \Delta t_{p+1}^{j_{ns}} - (t_{osp+1}^{new} - t_{osp+1})) & p < n_s \\ t_{wei} - t_{oei} & p = n_s \end{cases} \quad (A12)$$

where t_{oei} is the observation end time after target i is inserted into position p . Insertion position p is defined as the position where an unselected target i , between the selected target p and $p + 1$, is inserted. After target i is inserted into position p , the start time of observation mission $p + 1$ in the original sequence becomes

$$t_{osp+1}^{new} = t_{oep} + \Delta t_{Ap,i} + \Delta t_o + \Delta t_{Ai,p+1} \quad p < n_s. \quad (A13)$$

The sequence's backward time slack after target i is inserted into position p is $\Delta t_{lbs,i}^p$;

2. Determine whether the observation result sequence satisfies the attitude maneuver constraint after inserting an unselected target into the maximum sequence's backward time slack position. Subsequently, select the targets that satisfy the attitude maneuver constraint after the insertion. If the number of satisfied targets is more than 0, go to step 3, otherwise the calculation is finished;
3. Select target i and insertion position p that allows the sequence to obtain the maximum sequence's backward time slack after insertion. Insert target i at position p , update the observation result sequence, and remove target i from the unselected target set;
4. If the number of unselected targets is more than 0, return to step 1, otherwise the calculation is finished.

References

1. Zhang, B.; Wu, Y.; Zhao, B.; Chanussot, J.; Hong, D.; Yao, J.; Gao, L. Progress and Challenges in Intelligent Remote Sensing Satellite Systems. *IEEE J. Sel. Top. Appl. Earth Obs. Remote Sens.* **2022**, *15*, 1814–1822. [[CrossRef](#)]
2. Lin, M.S.; Jia, Y.J. Past, Present and Future Marine Microwave Satellite Missions in China. *Remote Sens.* **2022**, *14*, 16. [[CrossRef](#)]
3. Dial, G.; Bowen, H.; Gerlach, F.; Grodecki, J.; Oleszczuk, R. IKONOS satellite, imagery, and products. *Remote Sens. Environ.* **2003**, *88*, 23–36. [[CrossRef](#)]
4. Lamard, J.L.; Gaudin-Delrieu, C.; Valentini, D.; Renard, C.; Tournier, T.; Laherrere, J.M. Design of the high resolution optical instrument for the pleiades HR earth observation satellites. In Proceedings of the 5th International Conference on Space Optics (ICSO 2004), Toulouse, France, 30 March–2 July 2004; pp. 149–156.
5. Gu, X.F.; Tong, X.D. Overview of China Earth Observation Satellite Programs. *IEEE Geosci. Remote Sens. Mag.* **2015**, *3*, 113–129. [[CrossRef](#)]
6. Wang, J.J.; Song, G.P.; Liang, Z.; Demeulemeester, E.; Hu, X.J.; Liu, J. Unrelated parallel machine scheduling with multiple time windows: An application to earth observation satellite scheduling. *Comput. Oper. Res.* **2023**, *149*, 14. [[CrossRef](#)]
7. Lemaitre, M.; Verfaillie, G.; Jouhaud, F.; Lachiver, J.M.; Bataille, N. Selecting and scheduling observations of agile satellites. *Aerosp. Sci. Technol.* **2002**, *6*, 367–381. [[CrossRef](#)]
8. Peng, G.S.; Song, G.P.; Xing, L.N.; Gunawan, A.; Vansteenwegen, P. An Exact Algorithm for Agile Earth Observation Satellite Scheduling with Time-Dependent Profits. *Comput. Oper. Res.* **2020**, *120*, 15. [[CrossRef](#)]
9. Zhang, B.; Chen, Z.; Peng, D.; Benediktsson, J.A.; Liu, B.; Zou, L.; Li, J.; Plaza, A. Remotely sensed big data: Evolution in model development for information extraction point of view. *Proc. IEEE* **2019**, *107*, 2294–2301. [[CrossRef](#)]
10. Zhang, G.; Li, X.; Hu, G.; Zhang, Z.; An, J.; Man, W. Mission Planning Issues of Imaging Satellites: Summary, Discussion, and Prospects. *Int. J. Aerosp. Eng.* **2021**, *2021*, 7819105. [[CrossRef](#)]
11. Xie, P.; Wang, H.; Chen, Y.; Wang, P. A Heuristic Algorithm Based on Temporal Conflict Network for Agile Earth Observing Satellite Scheduling Problem. *IEEE Access* **2019**, *7*, 61024–61033. [[CrossRef](#)]
12. Grasset-Bourdel, R.; Flipo, A.; Verfaillie, G. Planning and replanning for a constellation of agile Earth observation satellites. In Proceedings of the 21th International Conference on Automated Planning and Scheduling (ICAPS 2011), Freiburg, Germany, 11–16 June 2011; p. 29.
13. Wang, X.-W.; Chen, Z.; Han, C. Scheduling for single agile satellite, redundant targets problem using complex networks theory. *Chaos Solitons Fractals* **2016**, *83*, 125–132. [[CrossRef](#)]
14. Wang, P.; Gao, P.; Tan, Y. A Model, a Heuristic and a Decision Support System to Solve the Earth Observing Satellites Fleet Scheduling Problem. In Proceedings of the International Conference on Computers and Industrial Engineering (CIE39), Troyes, France, 6–9 July 2009; pp. 256–261.
15. Sun, H.; Xia, W.; Wang, Z.; Hu, X. Agile Earth Observation Satellite Scheduling Algorithm for Emergency Tasks Based on Multiple Strategies. *J. Syst. Eng.* **2021**, *30*, 626–646. [[CrossRef](#)]
16. Liang, J.; Zhu, Y.H.; Luo, Y.Z.; Zhang, J.C.; Zhu, H. A precedence-rule-based heuristic for satellite onboard activity planning. *Acta Astronaut.* **2021**, *178*, 757–772. [[CrossRef](#)]
17. Baek, S.-W.; Han, S.-M.; Cho, K.-R.; Lee, D.-W.; Yang, J.-S.; Bainum, P.M.; Kim, H.-D. Development of a scheduling algorithm and GUI for autonomous satellite missions. *Acta Astronaut.* **2011**, *68*, 1396–1402. [[CrossRef](#)]

18. Liu, X.; Laporte, G.; Chen, Y.; He, R. An adaptive large neighborhood search metaheuristic for agile satellite scheduling with time-dependent transition time. *Comput. Oper. Res.* **2017**, *86*, 41–53. [[CrossRef](#)]
19. Du, B.; Li, S.; She, Y.; Li, W.; Liao, H.; Wang, H. Area targets observation mission planning of agile satellite considering the drift angle constraint. *J. Astron. Telesc. Instrum. Syst.* **2018**, *4*, 047002. [[CrossRef](#)]
20. Cui, K.; Xiang, J.; Zhang, Y. Mission planning optimization of video satellite for ground multi-object staring imaging. *Adv. Space Res.* **2018**, *61*, 1476–1489. [[CrossRef](#)]
21. Hao, H.; Jiang, W.; Li, Y. Improved algorithms to plan missions for agile earth observation satellites. *J. Syst. Eng. Electron.* **2014**, *25*, 811–821. [[CrossRef](#)]
22. Barkaoui, M.; Berger, J. A new hybrid genetic algorithm for the collection scheduling problem for a satellite constellation. *J. Oper. Res. Soc.* **2020**, *71*, 1390–1410. [[CrossRef](#)]
23. Zhang, J.W.; Xing, L.N. An improved genetic algorithm for the integrated satellite imaging and data transmission scheduling problem. *Comput. Oper. Res.* **2022**, *139*, 11. [[CrossRef](#)]
24. Zhou, Z.B.; Chen, E.M.; Wu, F.; Chang, Z.X.; Xing, L.N. Multi-satellite scheduling problem with marginal decreasing imaging duration: An improved adaptive ant colony algorithm. *Comput. Ind. Eng.* **2023**, *176*, 12. [[CrossRef](#)]
25. Long, W.J. Medical informatics: Reasoning methods. *Artif. Intell. Med.* **2001**, *23*, 71–87. [[CrossRef](#)]
26. Moulin, B.; Irandoust, H.; Belanger, M.; Desbordes, G. Explanation and argumentation capabilities: Towards the creation of more persuasive agents. *Artif. Intell. Rev.* **2002**, *17*, 169–222. [[CrossRef](#)]
27. Gayathri, R.; Uma, V. Ontology based knowledge representation technique, domain modeling languages and planners for robotic path planning: A survey. *ICT Express* **2018**, *4*, 69–74. [[CrossRef](#)]
28. Wu, X.J.; Tang, J.; Li, Q.; Heng, K.H. A vector-format fuzzy logic approach for online robot motion planning in 3D space and its application to underwater robotic vehicle. *Robotica* **2007**, *25*, 325–339. [[CrossRef](#)]
29. Vilchis-Medina, J.-L.; Godary-Dejean, K.; Lesire, C. Autonomous Decision-Making With Incomplete Information and Safety Rules Based on Non-Monotonic Reasoning. *IEEE Robot. Autom. Lett.* **2021**, *6*, 8357–8362. [[CrossRef](#)]
30. Martins, L.S.; Prajoux, R. Locomotion control of a four-legged robot embedding real-time reasoning in the force distribution. *Robot. Auton. Syst.* **2000**, *32*, 219–235. [[CrossRef](#)]
31. Abiyev, R.H.; Akkaya, N.; Gunsul, I. Control of Omnidirectional Robot Using Z-Number-Based Fuzzy System. *IEEE Trans. Syst. Man Cybern. -Syst.* **2019**, *49*, 238–252. [[CrossRef](#)]
32. Song, Y.; Xing, L.; Wang, M.; Yi, Y.; Xiang, W.; Zhang, Z. A knowledge-based evolutionary algorithm for relay satellite system mission scheduling problem. *Comput. Ind. Eng.* **2020**, *150*, 106830. [[CrossRef](#)]
33. Tinker, P.; Fox, J.; Green, C.; Rome, D.; Casey, K.; Furmanski, C. Analogical and case-based reasoning for predicting satellite task schedulability. In *Case-Based Reasoning Research and Development, Proceedings*; MunozAvila, H., Ricci, F., Eds.; Lecture Notes in Artificial Intelligence; Springer-Verlag Berlin: Berlin, Germany, 2005; Volume 3620, pp. 566–578.
34. Rojanasoonthon, S.; Bard, J. A GRASP for parallel machine scheduling with time windows. *INFORMS J. Comput.* **2005**, *17*, 32–51. [[CrossRef](#)]
35. He, R. Research on Imaging Reconnaissance Satellite Scheduling Problem. Ph.D. Thesis, National University of Defense Technology, Changsha, China, 2004.
36. Nanry, W.P.; Barnes, J.W. Solving the pickup and delivery problem with time windows using reactive tabu search. *Transp. Res. Pt. B-Methodol.* **2000**, *34*, 107–121. [[CrossRef](#)]
37. Bloechliger, I.; Zufferey, N. A graph coloring heuristic using partial solutions and a reactive tabu scheme. *Comput. Oper. Res.* **2008**, *35*, 960–975. [[CrossRef](#)]
38. Zhao, J.; Yang, F. *Agile Satellite*; National Defense Industry Press: Beijing, China, 2021.

Disclaimer/Publisher’s Note: The statements, opinions and data contained in all publications are solely those of the individual author(s) and contributor(s) and not of MDPI and/or the editor(s). MDPI and/or the editor(s) disclaim responsibility for any injury to people or property resulting from any ideas, methods, instructions or products referred to in the content.